Title

Water-assisted strong underwater adhesion via interfacial water removal and self-adaptive gelation.

Journal

Proceedings of the National Academy of Sciences of USA, 120(31)

Authors

Zhou, Feng
Qin, Chenxi
Ma, Yanfei
et al.

Publication Date

2023-08-01

DOI

10.1073/pnas.2301364120

Peer reviewed

PNAS RESEARCH ARTICLE | APPLIED PHYSICAL SCIENCES OPEN ACCESS

Water-assisted strong underwater adhesion via interfacial water removal and self-adaptive gelation

Chenxi Qin[a,b], Yanfei Ma[a,c,1], Zhizhi Zhang[a,b], Yingjie Du[d], Sidi Duan[d], Shuanhong Ma[a,c], Xiaowei Pei[a], Bo Yu[a], Meirong Cai[a,c], Ximin He[d,1], and Feng Zhou[a,1]

Edited by David Weitz, Harvard University, Cambridge, MA; received January 25, 2023; accepted June 30, 2023

In nearly all cases of underwater adhesion, water molecules typically act as a destroyer. Thus, removing interfacial water from the substrate surfaces is essential for forming super-strong underwater adhesion. However, current methods mainly rely on physical means to dislodge interfacial water, such as absorption, hydrophobic repulsion, or extrusion, which are inefficient in removing obstinate hydrated water at contact interface, resulting in poor adhesion. Herein, we present a unique means of reversing the role of water to assist in realizing a self-strengthening liquid underwater adhesive (SLU-adhesive) that can effectively remove water at contact interface. This is achieved through multiscale physical–chemical coupling methods across millimeter to molecular levels and self-adaptive strengthening of the cohesion during underwater operations. As a result, strong adhesion over 1,600 kPa (compared to ~100 to 1,000 kPa in current state of the art) can be achieved on various materials, including inorganic metal and organic plastic materials, without preloading in different environments such as pure water, a wide range of pH solutions (pH = 3 to 11), and seawater. Intriguingly, SLU-adhesive/photothermal nanoparticles (carbon nanotubes) hybrid materials can significantly reduce the time required for complete curing from 24 h to 40 min using near-infrared laser radiation due to unique thermal-response of the chemical reaction rate. The excellent adhesion property and self-adaptive adhesion procedure allow SLU-adhesive materials to demonstrate great potential for broad applications in underwater sand stabilization, underwater repair, and even adhesion failure detection as a self-reporting adhesive. This concept of "water helper" has potential to advance underwater adhesion and manufacturing strategies.

adhesive | underwater adhesion | self-adaptive | interfacial water | hydrated water

Water is seldom considered a "helper" in the adhesion process as it tends to prevent close contact at interfaces and reduce intermolecular interactions between the adhesive and the substrate, greatly limiting the development of strong underwater adhesion (1–5). Therefore, removing water molecules from the adhesive interface has become one of the most critical and challenging imperatives in designing high-performance underwater adhesives. Prominent progress has been made in achieving robust interface adhesion by removing interfacial water at different length scales through absorption, hydrophobic repulsion, and extrusion (3–6). At the micrometer to millimeter scale, surface microstructure and preload are effective strategies for facilitating the drainage of bulk water at the contact interface and preventing permanent water accumulation. At the molecular level, hydrophobic monomers and polymers are found to have good ability to remove interfacial water layer and promote surface wetting (especially for hydrophobic matrices). In addition, it is also effective to use water-absorbing fillers (including inorganic substances and hydrophilic polymers) to achieve this goal (2, 3). However, these physical dehydration methods cannot completely remove the interfacial water, especially hydration water, which is an ultrathin layer of interfacial water molecules existing between the adhesive material and the substrate surface. This is a critical factor in preventing ultrastrong adhesion and is notoriously difficult to remove (1–3, 5–8). Therefore, it is believed that truly complete interfacial water removal may require synergistic interfacial dehydration across multiple length scales (2).

The excellent mechanical property of adhesives is another important factor for avoiding cohesive failure (2, 7). Over the past decades, many methods for strengthening the cohesion of adhesives have been developed, including electrostatic interactions (8), hydrogen bonding (9), metal coordination (10), hydrophobic interactions (5), host–guest interactions (11), and covalent interactions (4). Although these strategies are effective in enhancing the cohesion, they generally require dry curing prior to immersion, the application of compressive pressure, assistance from external energy (e.g., temperature, light, ions, and pH), or long curing times (2 to 48 h) (2, 4, 12–14). These complex, cumbersome, and

Significance

Interfacial hydrated water is an obstacle to underwater adhesion but is challenging to remove. Here, for a self-strengthening liquid underwater adhesive (SLU-adhesive), a multiscale dehydration mechanism based on a physical–chemical coupling is utilized to achieve fast and robust underwater adhesion through deep-water removal at the contact interface and self-adaptive cohesion enhancement. The adhesion mechanism involves multiscale dehydration in three steps: 1) physical replacement at a millimeter scale: Surface water on the substrate tends to be replaced by the SLU-adhesive because of its excellent wettability and spreadability; 2) physical removal at a micrometer scale: Chemical reaction of the isocyanate groups with water releases lots of bubbles to remove interfacial water; and 3) chemical consumption of surface-bound water at a molecular level.

Author contributions: C.Q., Y.M., and F.Z. designed research; C.Q. and Z.Z. performed research; Y.M., S.M., X.P., B.Y., and M.C. contributed new reagents/analytic tools; C.Q., Y.M., X.H., and F.Z. analyzed data; and C.Q., Y.M., Z.Z., Y.D., S.D., X.H., and F.Z. wrote the paper.

The authors declare no competing interest.

This article is a PNAS Direct Submission.

[1]To whom correspondence may be addressed. Email: mayanfei@licp.cas.cn, ximinhe@ucla.edu, or zhouf@licp.cas.cn.

This article contains supporting information online at https://www.pnas.org/lookup/suppl/doi:10.1073/pnas.2301364120/-/DCSupplemental.

Published July 24, 2023.

inconvenient requirements greatly limit the wide applicability of the adhesives in practical situations. Thus, it remains a significant challenge to directly and rapidly form strong adhesion during immersion (of substrates already soaked in water), without applying external force or energy. These needs call for mechanisms of rapidly forming strong adhesion through easy operation in water.

In recent years, since Zhao et al. first proposed the method of realizing underwater contact adhesion with polyelectrolyte complexes through solvent exchange in 2016 (8), many glue-type adhesives that are fully implemented in water have been extensively studied and well developed. These adhesives are liquid precursor solutions that are cured underwater and adhere through electrostatic complexation (15), hydrophobic self-aggregation (5, 16, 17), hydrogen bond interactions (18–20), cation–π interactions (12, 21–23), metal coordination (7), or chemical reaction (24, 25), greatly promoting the development of the easy-to-implement underwater adhesives with excellent adhesion (*SI Appendix*, Table S1). However, these physical water removal methods, self-aggregation/self-curing through weak molecular interactions and single chemical reaction methods underwater, do little to remove hydration water and increase the polymerization rate (2, 24, 26). Therefore, it would be highly advantageous to have underwater adhesives capable of effectively removing interfacial water and self-adaptively and quickly enhancing cohesion during underwater adhesion operations without drying and curing before immersion, external energy input, or applying compression pressure.

In contrast to the existing methods of eliminating interfacial water through physical means, such as hydrophobic repulsion, swelling absorption, and extrusion (3–6), we propose a multiscale dehydration method that couples physical and chemical approaches to thoroughly remove interfacial water. By introducing a chemical reaction with water, the obstinate hydration water can be completely removed at the molecular level, under the premise that the physical dehydration via solvent replacement and bubble drainage has already removed most of the bulk water at millimeter to micrometer scales. Synergistically, these methods can minimize the impact of interfacial water on adhesive contact. Moreover, the controllability of chemical reaction rates opens a door to breaking the inherent limit on the long-term curing time of current glue-type underwater adhesives (2). If successful, the strategies of consuming interfacial water, hydrophobic repulsion, swelling absorption, extrusion, and multiple couplings may readily lend themselves to a wealth of materials chemistries.

As current synthetic adhesives are normally undermined by moisture (8, 27), it is conceptually unique to turn water into a helper. The design of water-involved and water-triggered underwater adhesion helps deeply remove interfacial water and promotes cohesion, allowing for rapid and robust wet adhesion on broad choices of solid substrates in a process entirely immersed in water. As an additional self-reporting function beyond conventional adhesives, our adhesive can be also applied to damaged area as a failure indicator to monitor its adhesion state in real time when stress exceeds a certain limit.

Herein, we report a viable approach to fabricate a self-strengthening liquid underwater adhesive (SLU-adhesive) capable of achieving robust underwater adhesion by effectively removing water at the contact interface and self-adaptively enhancing cohesion during underwater adhesion operations. Into the adhesive material design, we introduce the isocyanate group, which can react with water and cross-link the polymers to promote the adhesive gelation. Such a water-involved chemical reaction simultaneously consumes the hydration water and strengthens the adhesion through cross-linking. The produced carbon dioxide also helps repel interfacial water, as observed experimentally. When applied onto an underwater substrate, the adhesive first spreads and self-aggregates instantly, accompanied by the dissipation/repulsion of bulk interfacial water with bubbles, the consumption of hydration water by chemical reaction, and the self-adaptive cohesion enhancement through gelation. Such a process has been tested and proven capable of forming record-high strong adhesion on a variety of materials ranging from inorganic metal materials to organic plastic materials in widely different environments, including pure water, solutions of pH = 3~11, and seawater, without having to preload or trigger any external conditions. The gelation speed of the SLU-adhesive can be further accelerated by hybridizing with carbon nanotubes (CNTs) to endow the adhesive with a unique response to temperature. Such an adhesive material is further demonstrated to have broad applicability in underwater sand stabilization, underwater repair, and real-time self-detection of its own adhesion state especially upon external force impact and adhesion failure. The presented strategy opens opportunities for thorough interfacial water removal and developing intelligent high-performance underwater adhesives.

Results

Design Principle of SLU-Adhesive. To achieve strong underwater adhesion with simple underwater operation, the designed adhesive must have the following abilities: i) underwater gelation or self-aggregation from liquid to solid to adaptively enhance the cohesive force and alleviate the needs of manual or external force/energy application and ii) removal of interfacial water to form intimate interfacial interactions at the molecular level, in addition to bulk water repulsion at the micron to millimeter level. Here, we designed a SLU-adhesive that is capable of user-friendly underwater operation. The SLU-adhesive is based on poly (phenoxyethyl methacrylate-co-isocyanatoethylacrylate-co-methoxyethyl acrylate) [p(PMA-IA-MEA)] prepared through free radical polymerization of three monomers: PMA, IA, and MEA. The linear macromolecule polymers in the liquid adhesive with hydrophobic chain segments and reactive chain segments (-NCO) are able to self-aggregate and gelate adaptively under water to form a cross-linked three-dimensional polymer network with a porous microstructure, which can enhance the adhesion strength of underwater glues (Fig. 1*B*) (2, 5, 8). The carbon–carbon double bond was utilized as a characteristic marker and grafted onto -NCO groups, finally resulting in the -NCO groups accounting for 11.2% of the SLU-adhesive by mol (^{1}H-NMR spectroscopy) (*SI Appendix*, Figs. S1 and S3). As shown in Fig. 1*A*, a droplet (7 μL) of adhesive solution achieved spontaneous and complete spreading across the polymethyl methacrylate (PMMA) substrate surface in water, forming a spreading adhesion layer within 1 s. After 5 s, the adhesive gradually gelled. In this process of contacting, spreading, wetting, and gelation of the adhesive on the substrate surface, there is a series of spontaneous, tacitly coordinated adhesion behaviors that self-adaptively achieve interface adhesion and cohesion enhancement, including the removal of interfacial water, the consumption of hydrated water, and self-adaptive covalent cross-linking (Fig. 1*B*). The thorough removal of surface water provides a platform for SLU-adhesive to form a strong interaction force (e.g., van der Waals interaction, hydrogen bond, π-π and hydrophobic interaction) with the substrate surface (*SI Appendix*, Figs. S5 and S6). To demonstrate the excellent underwater adhesion of SLU-adhesive, this liquid adhesive was extruded onto PMMA and iron (Fe) sheets through a syringe in water. The painted liquid pattern cured quickly and adhered firmly to the surface of the substrate without falling off even under violent water blasting (2 bar, 45 s) (Movie S1). This demonstration showed the potential of SLU-adhesive for direct use

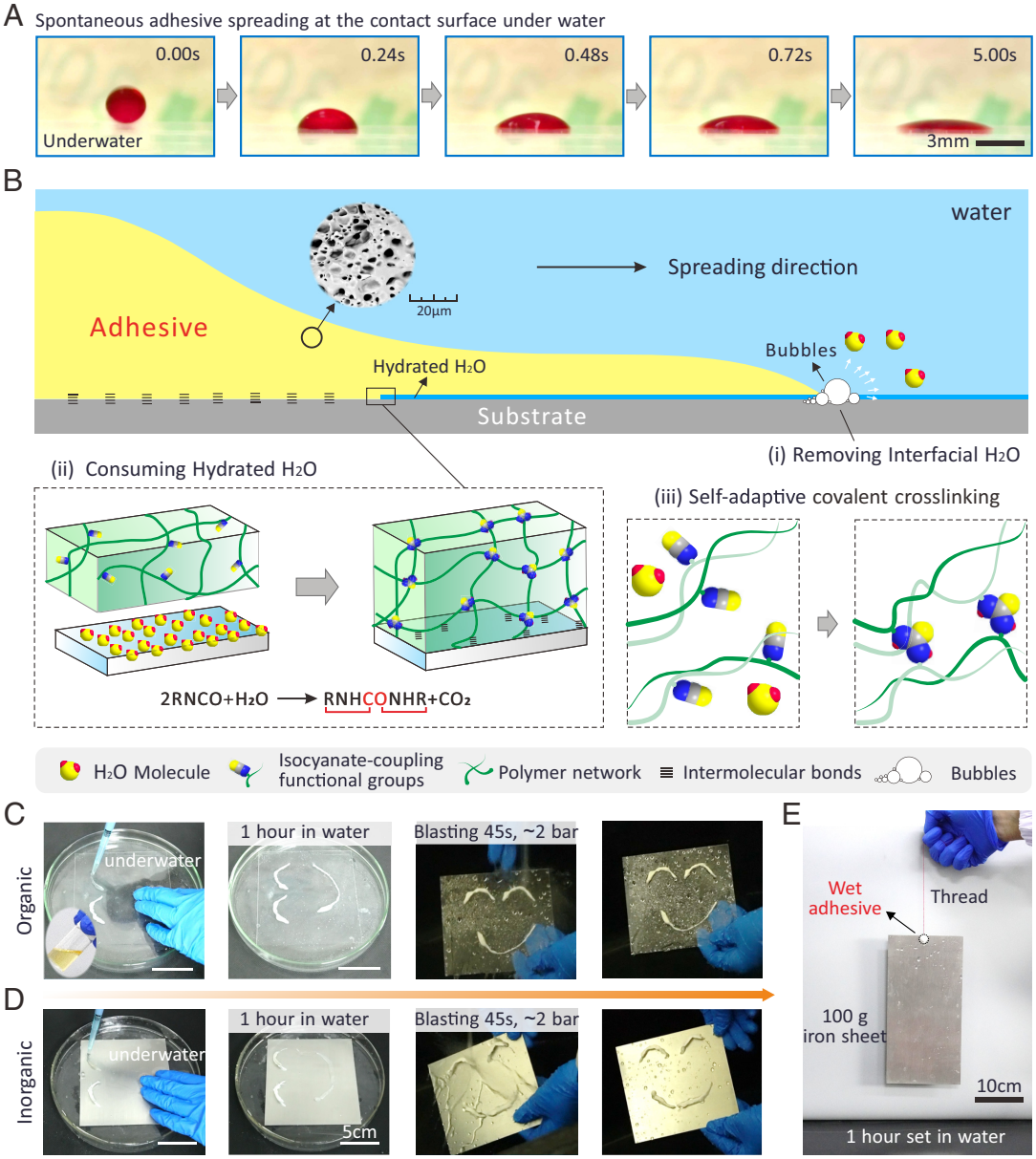

Fig. 1. Design and adhesion process of the SLU-adhesive. (*A*) A Sudan IV-stained adhesive droplet (7 μL) spontaneously wets PMMA substrate surface, forming a complete spreading adhesive layer. (*B*) The theoretical study and schematic diagram of the self-strengthening mechanism of water-induced adhesive in the spreading process. Scanning electron microscope (SEM) shows a sandcastle worm-like protein pore structure inside SLU-adhesive. (*C* and *D*) Digital images show the adhesion of SLU-adhesive to the organic (PMMA) and inorganic (Fe) surfaces under water. After being placed in water (20 °C, no applied pressure) for 1 h, the adhesion to different substrates withstood water blasting (2 bar, 45 s). (*E*) Adhesive polymer blend with embedded cotton thread casted onto an Fe sheet in water. After 1 h, adhesion force can support the weight (100 g) of the sheet in air.

in underwater operations (Fig. 1 *C* and *D*). Our adhesive exhibited excellent adhesion properties when a cotton rope was adhered to a submerged Fe sheet surface and withstood a 100-g load (Fig. 1*E*). This type of adhesion with self-adaptive adhesion can also bond two solids in water without the application of compressive force (*SI Appendix*, Figs. S11–S13).

Physical–Chemical Coupling Water Removal and Self-Adaptive Gelation. Traditional adhesives eliminate interfacial water based on physical water removal, such as hydrophobic repulsion, swelling absorption, and extrusion. Our adhesive distinguishes itself from traditional adhesives as a SLU-adhesive by achieving underwater adhesion with a physical (solvent exchange and bubbly drainage) and chemical (chemical reactions consume interfacial bound water) coupling water removal process. In order to verify the SLU-adhesive's self-adaptive adhesion procedure, we carried out mechanism research for adhesion in two aspects: enhancement of surface adhesion based on removal of interfacial water and improvement of cohesion via self-adaptive gelation. In this work, for SLU-adhesive, the removal of interfacial water is orderly divided into three steps: 1) physical replacement of the surface water on the substrate with SLU-adhesive at mm scale because of its excellent wettability; 2) physical removal of water at μm scale by generating carbon dioxide bubbles from the chemical reaction between isocyanate groups and water at the interface; and 3) simultaneous chemical consumption of the surface-bound water at molecular level. This series of adhesion behaviors is instantaneous, spontaneous, and tacitly coordinated throughout the entire process of liquid adhesive contact, spreading, wetting, and gelation on the substrate surface. Water and isocyanate groups

have very low reactivity (28, 29), most chemical reactions occur after "physical displacement". As shown in Fig. 2*A*, the contact angles of SLU-adhesive on various substrate surfaces (organic and inorganic) were all smaller than that of water. This implies that when the adhesive is applied to the substrate, the SLU-adhesive tends to replace interface water to achieve sufficient contact area on the substrate. Meanwhile, the chemical reaction of isocyanate chain segments with water releases a lot of bubbles to shield the boundary water layer around the adhesive, transforming the initial water/adhesive interface into water/gas/adhesive interface, achieving a similar dry state of adhesion, thus greatly enhancing the adhesion interaction. In order to verify the shielding of interfacial water by bubbles, we employed distinct fluorescent to label water and adhesive, respectively. Under the fluorescence microscope, SLU-adhesive containing 4-(1-pyrenyl) butyl methacrylate (PBMA) showed blue, while the water stained by Rhodamine B showed yellow (*SI Appendix*, Fig. S7). As shown in Fig. 2*B*, SLU-adhesive spread well on the fully immersed glass substrate surface, and the adhesive boundary was surrounded by a gas film formed from a large number of bubbles. The gas film shielded the adhesive from direct contact with the water and pushed away the surrounding water molecules as the adhesive spread (*SI Appendix*, Fig. S8 and Movie S2). In order to verify the complete removal ability of SLU-adhesives on the interface water, we employed sum frequency generation (SFG) spectroscopy to detect its dynamic interfacial dehydration behavior. As shown in Fig. 2*C*, the plasma-treated quartz surface exhibits a substantial water signal. In the measured spectral window where the OH stretches contribute two large peaks peak were observed, which we refer to as the 3,200- and 3,400-cm^{-1} modes (Fig. 2 *C*, *i*), which are attributed to interfacial water (30). As the interfacial water was removed by the SLU adhesive, the overall intensity of the SFG signal of the 3,200 and 3,400 cm^{-1} decreased dramatically within 30 s, approaching zero (Fig. 2 *C*, *ii*). At this time, the SFG signal in the interfacial water range disappears, which further proves the complete removal of the interface water (Fig. 2 *C*, *iii*). Interestingly, after the interfacial water was completely removed, we detected an obvious SFG signal from the benzene ring of SLU-adhesive, which means that the SLU-adhesive is in full contact with the substrate interface and adhesion has been achieved (Fig. 2 *C*, *iv*). In contrast, adhesives without isocyanate groups cannot completely remove interfacial water and achieve sufficient contact and effective adhesion (*SI Appendix*, Fig. S9). The chemical reaction was verified by Fourier transform infrared (FTIR) spectra, which monitored the Infrared absorption peaks of the adhesive before and after curing. Compared to the precure adhesive, the cured adhesive showed an absorption peak at 3,380 cm^{-1}, which was caused by -NH- groups, confirming the occurrence of cross-linking reactions in the adhesive. To further verify the ability of -NCO segment to remove hydrated water, the oxygen plasma-treated polyimide (PI) surfaces were wetted with H_2O and D_2O, respectively, and the bulk water on the surface was removed by air blowing, whereupon SLU-adhesive was dropped onto the H_2O and D_2O wetted PI surface to enhance adhesion. Proton NMR (^1H NMR) experiments were conducted on adhesives triggered by H_2O and D_2O. For H_2O-cured SLU-adhesive, the red line in Fig. 2*E* displayed its ^1H NMR spectrum in $CDCl_3$. The hydrogen spectrum signal in the RNHCONHR was clearly observed at 3.6 ppm. Correspondingly, the signal at 3.6 ppm disappeared in D_2O-cured adhesive samples, owing to the H being replaced by D in the RNDCONDR. In short, the self-adaptive adhesion procedure of replacing, removing, and consuming water achieves deep dehydration of the underwater substrate surface and thus endows SLU-adhesive with excellent surface adhesion strength. In addition, the cross-linking reaction also endows the SLU-adhesive with self-gelling ability and enhances its cohesion. The viscoelastic properties of the precured adhesive and the cured adhesive were evaluated by oscillatory rheometry. For precured adhesives, both storage modulus (G') and loss modulus (G") were extremely low and G" was higher than G', showing a liquid state. After curing, the obtained G' and G" greatly increased from 10^{-1} Pa to 10^5 Pa, where G' was higher than G", indicating that the cohesion of the liquid adhesive was rising and eventually resulted in the solid phase (Fig. 2*F*).

Underwater Adhesion Properties. To quantify the adhesion performance of SLU-adhesive, the lap shear test was performed to examine its underwater adhesion strength on various substrate materials placed in water for different time periods (Fig. 3 *A*–*C*). All operations were performed underwater without external load or any triggering from external sources (*SI Appendix*, Fig. S10). The results showed that SLU-adhesive formed coacervate in a relatively short period of time after contact with water and the cured adhesive could firmly adhere to diverse substrates. For PI, Titanium sheet (Ti), polyethylene (PE), Fe, aluminum (Al), PE terephthalate (PET), polypropylene (PP), wood, and PMMA, the underwater adhesion strengths of SLU-adhesive were 121.3, 106.6, 85.3, 52.6, 55.3, 49.3, 63.0, 151.6, and 83.3 kPa, respectively, after 10 min underwater. Increasing the curing time to 1.5 h allowed the adhesion strengths to increase to 234.3, 119.6, 184.3, 404.3, 112.6, 266.0, 139.3, 432.3, and 167.6 kPa, respectively (Fig. 3*B*). Finally, when the curing time in water was 12.5 h, the adhesion strength could reach up to 666.0, 1241.3, 210.6, 623.6, 608.0, 877.0, 245.3, 866.3, and 745.0 kPa, respectively (Fig. 3*C*). The prolongation of curing time allowed the internal cross-linking of the adhesive to reach sufficient levels, resulting in an increase in the adhesive strength. In addition, when PMMA was chosen as the adhesive substrate and the time was further extended to 96 h, there was no obvious change in the adhesion strength. Throughout the entire adhesion process, the adhesion strength gradually increased and finally reached a stable state at 12.5 h meaning complete gelation, which was correlated to the chemical reaction kinetics of the isocyanate group in SLU-adhesive (Fig. 3*D*). It is noted that the SLU-adhesive exhibited a robust adhesion ability to various materials without preload. What is more, adhesion strength of SLU-adhesive is solvent-dependent, with better performance achieved under dimethyl sulfoxide (DMSO) conditions (*SI Appendix*, Fig. S15). Based on this phenomenon, replacing the solvent with DMSO, the adhesion tests were performed on these above substrates, and the curing time in water was 12.5 h. The adhesion strength could reach up to 760.2, 1629.2, 288.2, 966.0, 770.6, 1056.0, 284.6, 1178.7, and 857.2 kPa, respectively (*SI Appendix*, Fig. S16). In addition, based on the superdehydration capability of SLU-adhesive, it can form mixed AB adhesives with other polar polymers to achieve stronger underwater adhesion properties beyond 2,000 kPa (400 N) (*SI Appendix*, Fig. S18).

To verify the adhesion performance of SLU-adhesive in harsh environments, adhesion tests were performed on immersed PI (organic) and Fe (inorganic) substrates in aqueous solutions with pH values ranging from 3.10 to 11.03. In these experiments, the sheets were bonded in different pH solutions and left to immerse for 12.5 h. The results showed that the adhesive had strong adhesion strength to the both organic and inorganic substrates across a wide pH range (pH 3.1~11.03). For Fe substrates, the adhesion strengths at pH = 3.10, 7.82, 8.97, 11.03 were 544.6, 453.0, 527.3, and 661.6 kPa, respectively. For PI substrates, the adhesion strengths were 503.0, 544.0, 503.6, and 415.3 kPa, respectively

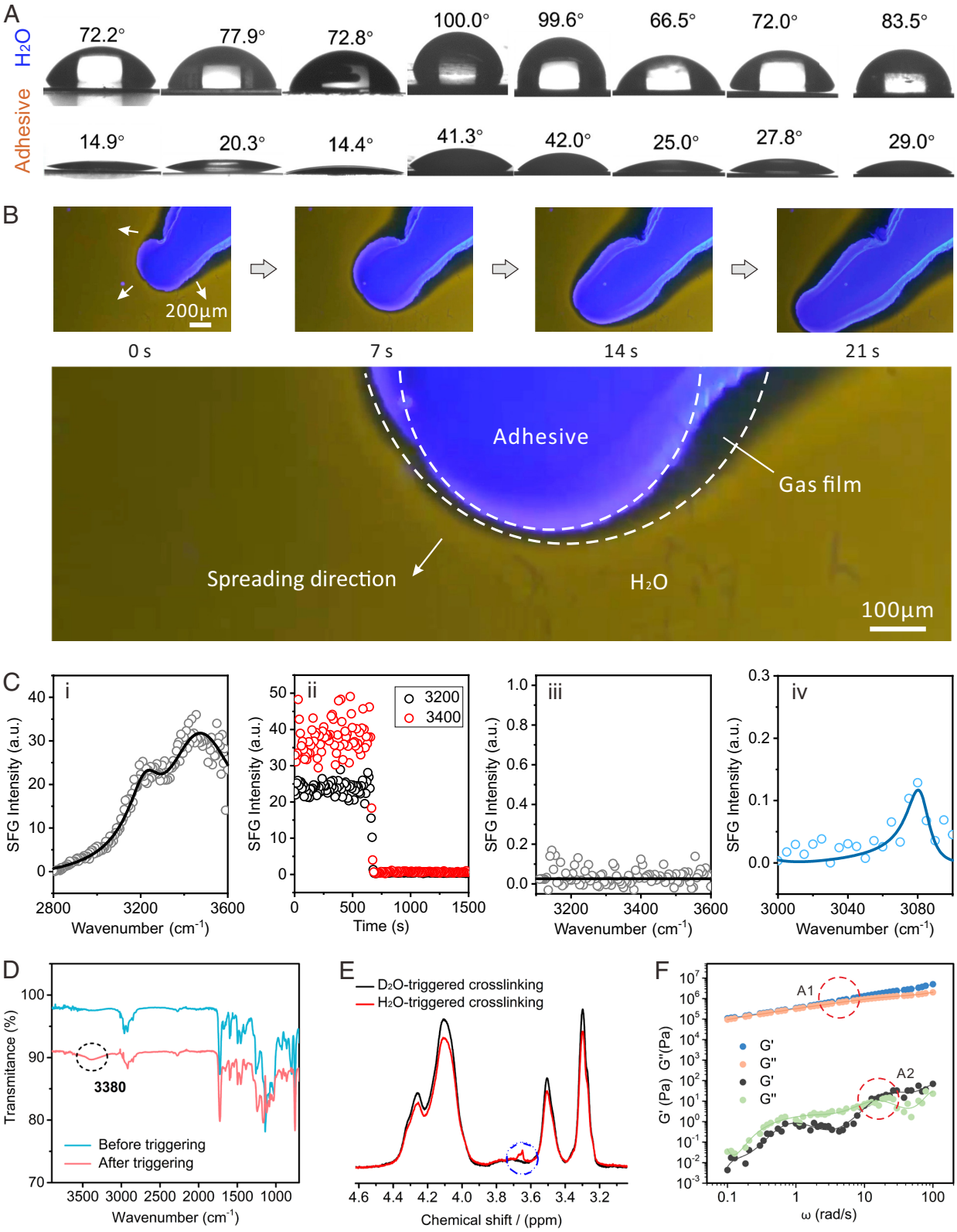

Fig. 2. The adhesion mechanism of SLU-adhesive in the spreading process. (*A*) Contact angles of SLU-adhesive and water on different substrates (from *Left* to *Right*: respectively, PI, PET, PMMA, PE, PP, aluminum sheet, Titaniumsheet and Fe sheet. Above: water, below: adhesive). (*B*) Dynamic process of gas film removing the interfacial water. (*C*) The process of dynamic dehydration of SLU-adhesive at the adhesion interface detected by SFG spectroscopic system: (*i*) SFG spectrum of interfacial water on a plasma-treated quartz surface, (*ii*) time-dependent SFG intensities at 3,200 and 3,400 cm^{-1}, (*iii*) SFG spectra of interfacial water after SLU-adhesive contacts with quartz surface, (*iv*) SFG spectra of quartz surface after SLU-adhesive forms adhesion with quartz surface. (*D*) FTIR of SLU-adhesive before and after gelation. (*E*) ^{1}H-NMR spectra of the adhesives triggered by bound D_2O and H_2O on the PI surface by plasma treatment. (*F*) Rheological behaviors of SLU-adhesive before (A2) and after gelation (A1).

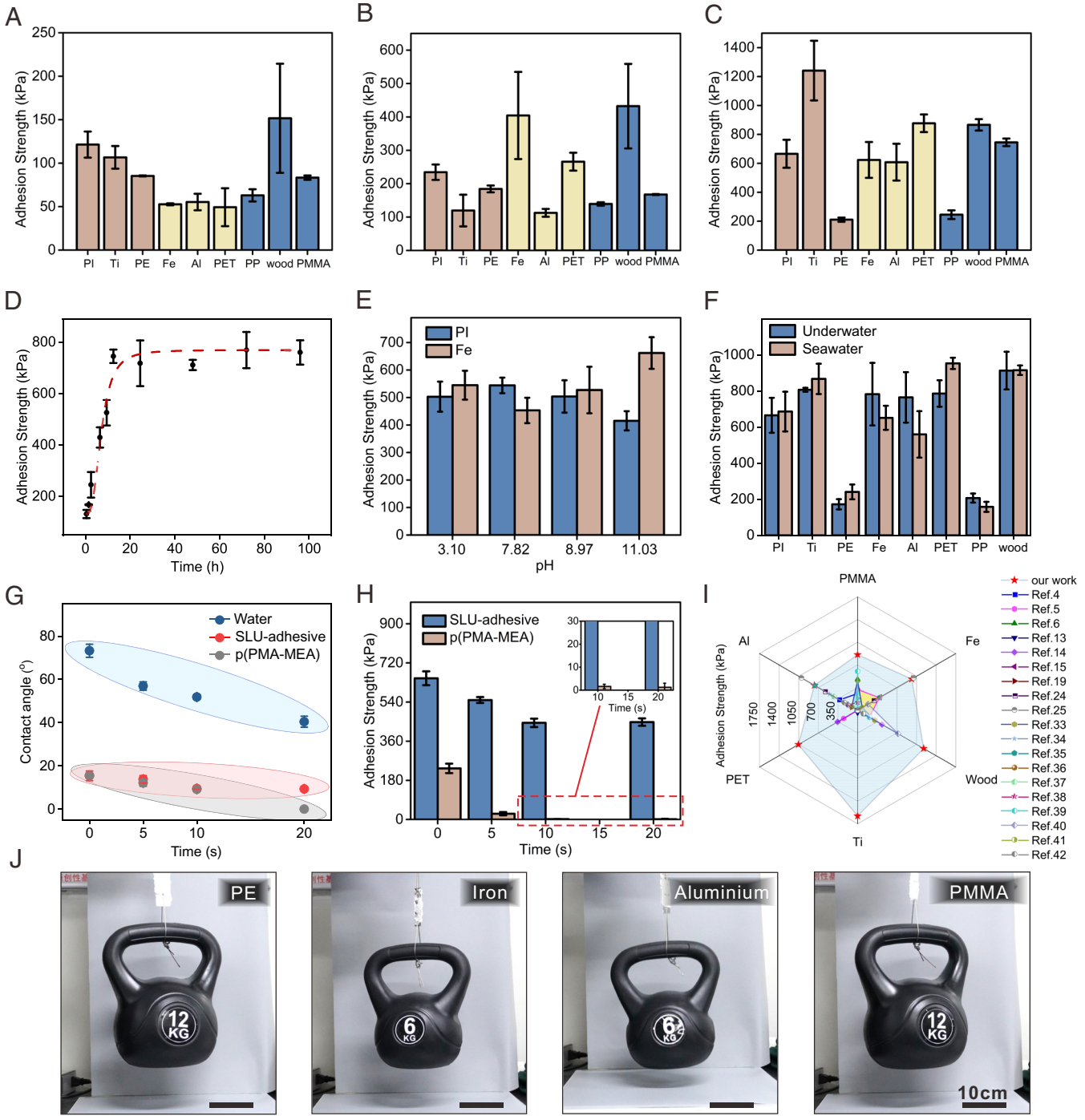

Fig. 3. The underwater adhesion performance of the SLU-adhesive. (*A–C*) Adhesion strengths of SLU-adhesive to different substrates after soaking in water for 10 min, 1.5 h, and 12.5 h. (*D*) The relationship between the adhesion strength to PMMA and the soaking time. (*E*) Adhesion strengths of SLU-adhesive to Fe and PI sheets after soaking in different pH media for 12.5 h. (*F*) Adhesive strengths of SLU-adhesive to different substrates after soaking in artificial seawater for 24.5 h. (*G*) Relationship between the wettability of PI surface and plasma treatment time. (*H*) Relationship between adhesion strength to PI surface and plasma treatment time. (*I*) Comparison of adhesion strengths of SLU-adhesive to PET, PMMA, Fe, wood, Ti and Al with the literature values of adhesives that can be operated underwater. (*J*) Macroscopic adhesion tests of SLU-adhesive on various substrates (the adhesion areas are 19.4, 6.0, 6.0, and 6.1 cm^2 on PE, Fe, Al and PMMA, respectively).

(Fig. 3*E*). To further explore the adhesion properties of the SLU-adhesive in more complex and practical application environments (e.g., alkaline and saline environments), the various substrates were left in artificial seawater for 24.5 h to achieve bonding operations. The resulting adhesion strengths of the SLU-adhesive on PI, Ti, PE, Fe, Al, PET, PP, and wood surfaces were 686.6, 868.0, 241.0, 652.0, 560.3, 954.3, 158.0 and 916.3 kPa, respectively. All substrates exhibited stable and excellent adhesion strength with our adhesive (Fig. 3*F*). Furthermore, we evaluated the thermal tolerance of the SLU-adhesive at various temperatures and observed that the adhesion strength did not decrease at low or high temperatures (*SI Appendix*, Fig. S14). We demonstrate in Fig. 2 that the outstanding adhesion properties of SLU-adhesive resulted from its ability to remove and consume interfacial hydrated water during the adhesion process. To verify the excellent dehydration ability of SLU-adhesive, PI treated with surface oxygen plasma (100 W) was

used as a substrate to test the adhesion strength of SLU-adhesive. p(PMA-MEA) was used as a control sample. As shown in Fig. 3*G*, with the increase in oxygen plasma time, the wettability of SLU-adhesive [p(PMA-MEA-IA)] and p(PMA-MEA) on the PI substrate surfaces improved. This is caused by the enhancement of –OH group density on the polymer surface with the increasing oxygen plasma time, where the hydroxyl groups on the treated surface and hydroxyl groups of water could be exchanged to form bounded water (31, 32). Although increasing the wettability of an adhesive on the substrate surface will improve interfacial adhesion, it is still futile for highly hydrated surfaces. As shown in Fig. 3*H*, for control samples p(PMA-MEA) without deep dehydration ability, the increase in surface hydration severely disrupted the interfacial adhesion, so that adhesion strength decreased from 235 to 1.25 kPa. By contrast, SLU-adhesive showed negligible decrease, which further proved that high adhesion force derived from the isocyanate-coupling functional groups in SLU-adhesive.

In conclusion, the SLU-adhesive can achieve a high bonding strength with adhesive mechanisms that can be easily realized even in an entirely underwater process and is compatible with a variety of materials. Notably, it exhibited better adhesion strength in water with PMMA, Fe, wood, Ti, and Al substrates than most recent underwater adhesives in the state of the art (Fig. 3*I*, and details in *SI Appendix*, Table S1) (4–6, 13–15, 19, 24, 25, 33–42). Fig. 3*J* displays the macroadhesion photos in air after SLU-adhesive was adhered to different substrates underwater and placed for 24 h in water. For PMMA substrate material, the 12-kg kettlebell could be easily lifted without separation or dislocation observed (the adhesion area was 14.78 mm × 41.41 mm). Such excellent adhesion was also observed on many other substrates, e.g., Fe, Al, and PE.

Traditional glue-type adhesives generally require ineluctable long curing times. Unfortunately, their curing rate can be difficult to increase due to their inherent polymerization mechanism, such as electrostatic complexation, hydrophobic self-aggregate, hydrogen bond interaction, cation–π interactions, etc. (2). The curing and gelling process of SLU-adhesive originates from the chemical reaction of isocyanate groups and interfacial water, and increasing the temperature will speed up the reaction rate, thus effectively controlling the gelation time (43). As shown in Fig. 4*A*, adhesion strength to PI substrate increased with temperature. As shown in *SI Appendix*, Fig. S20, SLU-adhesive bonding with PI substrates could reach maximum adhesion strength of ~600 kPa after soaking in 80 °C water for 40 min (adhesion strength comparable to 24 h at room temperature), which was better than most polymer solution type underwater adhesives (Fig. 4*F*). To enable a localized and remote-controlled adhesion enhancement, we incorporated photothermal multiwalled CNTs (MWCNTs) into SLU-adhesive to fabricate the MWCNTs/SLU-adhesive (Fig. 4*B*). Fig. 4*C* shows that there is good compatibility between MWCNTs and SLU-adhesive, which is also the basis for introducing MWCNTs to accelerate the adhesion speed without sacrificing the adhesion properties. It is noteworthy that the doping of a very small amount (0.05 to 0.2 wt%) of MWCNTs in SLU-adhesive accelerates the curing rate, leading to high adhesion strength in a short period of time. Specifically, introducing 0.2 wt% MWCNTs into SLU-adhesive could lead to an adhesion strength of 405.3 kPa after exposure to near-infrared light (NIR) for 12 min. This clearly indicates that the high temperature accelerated the cross-linking reaction inside SLU-adhesive because of the photo-thermal effect of MWCNTs (*SI Appendix*, Fig. S19). When irradiating the

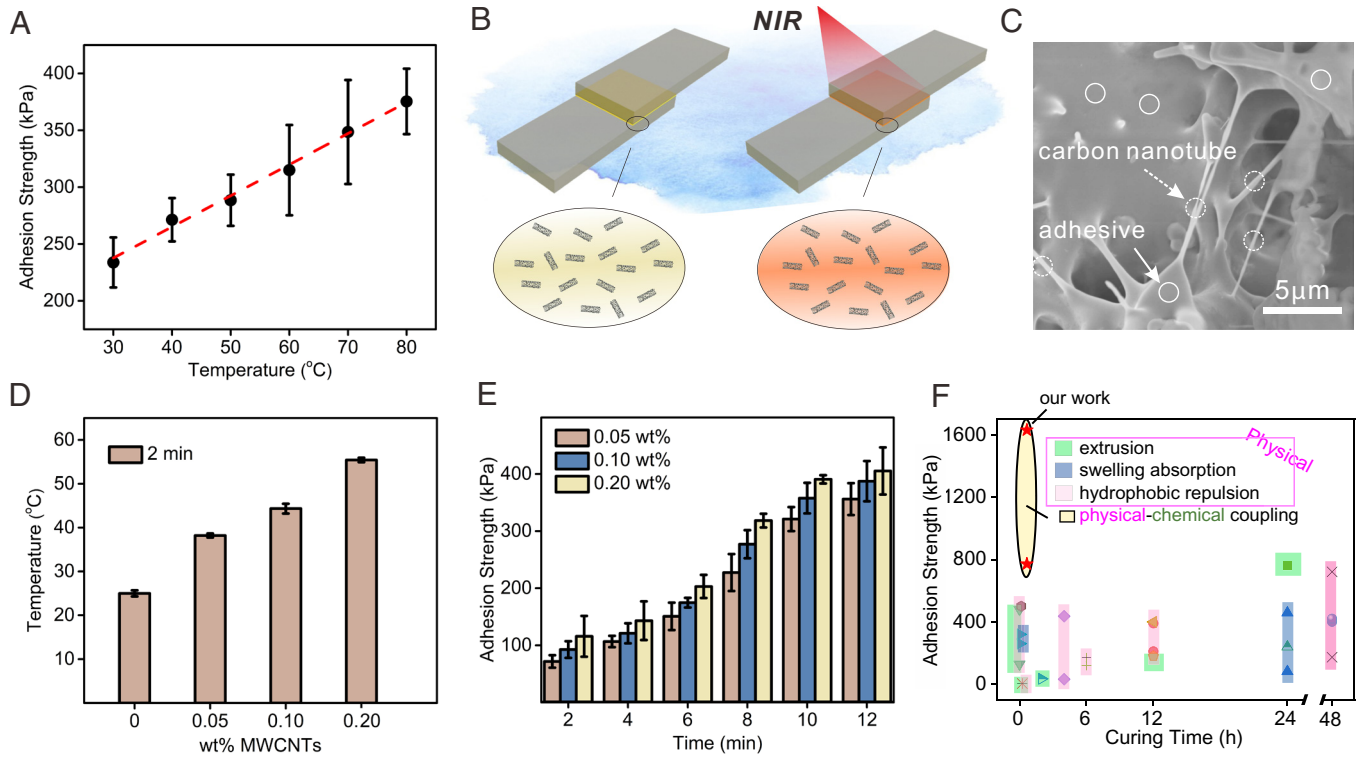

Fig. 4. Engineering MWCNTs/SLU-adhesive and realizing photo-controlled enhancement of adhesion strength by NIR irradiation. (*A*) Temperature-dependent adhesion strength tests of SLU-adhesive to PI substrate materials for 10 min. (*B*) Photocontrolled enhancement of adhesion strength of SLU-adhesive by the photothermal effect of MWCNTs. (*C*) Scanning electron microscope (SEM) image shows the distribution of doped MWCNTs (0.2 wt%) in the MWCNTs/SLU-adhesive. (*D*) Local temperature changes of the MWCNTs/SLU-adhesive (0%, 0.05%, 0.1%, 0.2 wt% MWCNTs) after irradiation in water for 2 min. (*E*) With the change of MWCNTs content and irradiation time, the adhesion strength of MWCNTs/SLU-adhesive changed. (*F*) Comparison of underwater adhesion strength, curing time, and methods to eliminate interfacial water of adhesives that can be operated underwater reported in the literature (4–6, 13–15, 19, 24, 25, 33–42).

adhesive containing 0.05 wt% MWCNTs, the temperature could reach 38.3 °C within 2 min (Fig. 4*D*). Further increasing the MWCNTs content (e.g., 0.2 wt%) or extending the exposure time (e.g., 12 min) could magnify the photothermal effect, thus reducing curing time for high adhesion strength (*SI Appendix*, Fig. S23 and Fig. 4*E*). In short, the controllability of chemical reaction rates opens a door to breaking the inherent limitation of traditional glue-type underwater adhesives that require long-term curing.

Applications of SLU-Adhesive. Owing to its simplicity and versatility, the self-adaptive adhesion system and SLU-adhesive with deep removal of interfacial water and self-adaption gelation has potential applications underwater engineering and intelligent sensors. For example, similar to the function of plant roots, SLU-adhesive could be used as wet soil or sand-adhering material to fix loose soil or sand in water due to its excellent fluidity, wettability, and underwater adhesion (Fig. 5*A*). As shown in Fig. 5*B*, SLU-adhesive was dripped into sand submerged in water. With the flow, penetration, and wetting of the liquid adhesive, most of the sand grains were encapsulated by the adhesive. After 24 h, the agglomerated sand could be lifted by cotton threads stuck in the sand without loose sand falling off (Movie S3). The result indicates that the fixation of loose sand by SLU-adhesive can be easily achieved through water-induced coagulation and solidification without any external stimulation. This property can be utilized in many potential applications, such as underwater quicksand tunnels where sand fixation is required, and the shores of artificial islands, where sand needs fixation to prevent seawater erosion. What is more, it is also evident that the SLU-adhesive exhibits excellent adhesion strength to nonideal (rough) surfaces commonly seen in real-world scenarios, thus has great potential for practical applications (Fig. 5*C*). The fast and strong in-situ adhesion properties of SLU-adhesive make it convenient and reliable for use in underwater engineering. As shown in Fig. 5*D*, MWCNTs/cotton/SLU-adhesive hybrid material was successfully used to repair damaged boats. To illustrate this process, we drilled nine-round holes (diameter = 0.4 cm) into the wooden boat

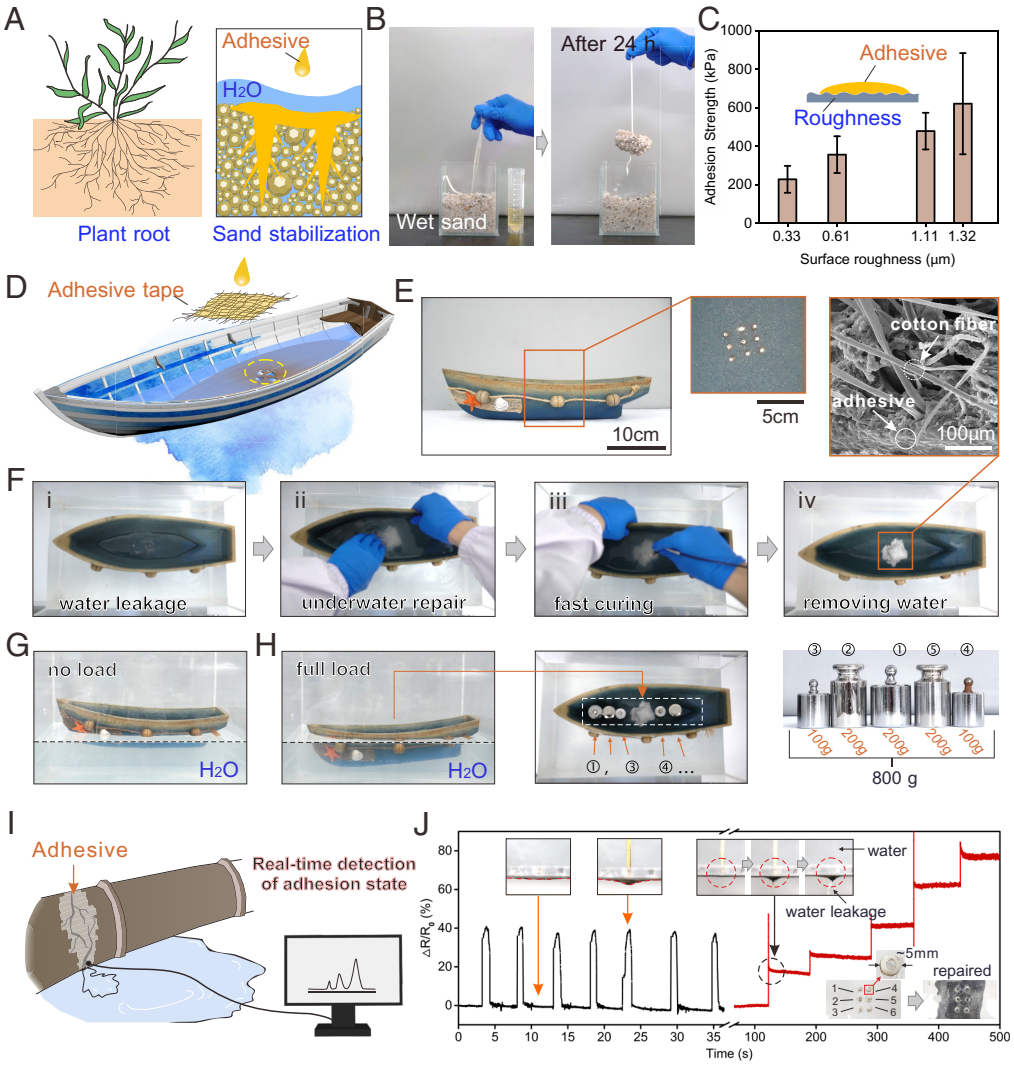

Fig. 5. Multifunctional application of SLU-adhesive and its composites. (*A*) SLU-adhesive was used for underwater sand stabilization, mimicking the hyperbranched root system of plants. (*B*) SLU-adhesive was dripped into wet sand surface, and the sand fixation was achieved after 24 h through the processes of wetting, penetration, diffusion, and self-gelling. (*C*) The effect of surface roughness on adhesion strength of SLU-adhesive. (*D*) Application of underwater repair of a damaged hull. (*E*) The damaged boat with 9 holes in the *Bottom*. (*F*) Repair process of the boat based on MWCNTs/SLU-adhesive doped with cotton fibers: (*i*) water leakage, (*ii*) underwater repair, (*iii*) fast curing, (*iv*) removing water. (*G* and *H*) Empty and full-load states of the repaired boat on the water. (*I*) Highly sensitive conductivity of MWCNTs/SLU-adhesive/PE film composites as smart electronic adhesives to achieve real-time detection of its own adhesion state. (*J*) The resistance response when the hole repaired by the adhesive was impacted and damaged by an external force.

and placed it on the water (Fig. 5*E*). Then water was poured into the wooden boat through the holes and the boat started to sink (Fig. 5 *F*, *i*). Afterward, we used MWCNTs/cotton/SLU-adhesive hybrid material to repair the damaged part of the boat underwater (Fig. 5 *F*, *ii*). After 10 min of NIR irradiation to accelerate curing (Fig. 5 *F*, *iii*), the damaged hull was repaired, and the water seeping into the boat was removed (Fig. 5 *F*, *iv*). The repaired boat was then placed into the water again and was capable of floating without any water leaking through the sealed holes (Fig. 5*G*). To further verify the stability of the repaired boat under full-load conditions, a weight of 800 g was placed inside the wooden boat, and the damaged areas were checked for water seepage (Fig. 5*H*). The result showed that the MWCNTs/cotton/SLU-adhesive hybrid material still firmly adhered to the damaged regions and no water penetrated into the wooden boat (Movie S4). For hulls, pipelines, and other objects that are subject to high shock pressure, the repaired parts are most prone to accidents. Therefore, it is very important to detect and monitor the stability of the maintenance site in real time. Most real-time monitoring requires additional complex detection systems, which also greatly limits the monitoring of complex and large numbers of adhesion sites. Here, SLU-adhesive can also be used as a sensing material to monitor its adhesion state in real time, which will facilitate the detection of repaired sites. Specifically, double-sided adhesive materials of MWCNTs/SLU-adhesive/PE/MWCNTs/SLU-adhesive were used for underwater repairing and real-time detection of adhesion state (Fig. 5*I* and *SI Appendix*, Fig. S22). The $\Delta R/R_0$ of the hybrid adhesive materials exhibited an increasing trend with the impact of external force, which might be related to the adhesive deformation (44). Meanwhile, it was found that the resistance could smartly drop back to the original value after releasing the strain, showing excellent strain-dependent recoverability. Once the adhered material was damaged under the impact of external force, the $\Delta R/R_0$ of the material would increase rapidly and could not be recovered, which might be related to its plastic deformation. As shown in Fig. 5*J*, when the repaired 6 holes were successively damaged under the impact of external force, their corresponding $\Delta R/R_0$ also increased step by step.

Conclusion

In summary, we have developed a high-performance liquid adhesive material that can perform adhesion operations underwater. Based on a series of self-adaptive adhesion procedures, including replacing, removing, consuming interfacial water, and self-gelling, SLU-adhesive achieves strong underwater adhesion strength to various materials, including inorganic metal materials and organic plastic materials, in different environments, such as pure water, a wide range of pH solutions (pH = 3 to 11) and seawater, without any preload or external trigger. In this work, water acts as a helper instead of an obstacle. Moreover, different from traditional glue-type adhesives which require a long curing time, MWCNTs/SLU-adhesive is able to achieve robust and optimal adhesion under 40-min NIR light irradiation, which is also attributed to the positive correlation of underwater adhesion strength with temperature. This fast and remote in-situ underwater adhesion enhancement also facilitates its use in underwater engineering. We believe that this liquid underwater adhesive has potential and multipurpose applications in direct work bonding underwater, fixing scattered sand in water, underwater repairing, and underwater detection, etc. Also, this method of physical (bubbly drainage) and chemical (chemical reactions consume interfacial bound water) coupling water removal offers a platform for designing adhesives and functional adhesion materials.

Materials and Methods

Materials. PMA (85%, stabilized with hydroquinone (HQ) + monomethyl ether hydroquinone (MEHQ), TCI), IA (98%, stabilized with butylated hydroxytoluene (BHT), TCI), 1-pyrenebutanol (99%, Sigma-Aldrich), 2,2′-Azobis (isobutyronitrile) (AIBN, 99%, recrystallization, Aladdin, Shanghai, China), MEA (98%, stabilized with 80 to 120 ppm MEHQ, J&K, Beijing, China) was passed through an alkaline Al_2O_3 column to remove inhibitor. 2-Hydroxyethyl methacrylate (HEMA, 99%, Anhydrous, stabilized with 200 ppm MEHQ, Aladdin, Shanghai, China), dibutyltin dilaurate (DBTDL, 97.5%, J&K, Beijing, China), carboxylic MWCNTs (MFCD00133992, Macklin, Shanghai, China), dichloromethane, N, N′-dimethylformamide (DMF), and n-hexane were purchased from Rionlon Bohua (Tianjin) Pharmaceutical Chemical Co. Ltd. Other regents were used without any purification. Deionized water was utilized in all processes.

Synthesis of PBMA (Fluorescent Monomer). 1-pyrenebutanol (0.28 g, 10 mmol) was dissolved in 10 mL dichloromethane and subsequently transferred into a light-shielded three-neck flask. The mixture was then placed in an ice bath and nitrogen gas was introduced for 30 min. Afterward, 0.17 mL triethylamine was added and stirred for another 30 min. Next, 0.18 mL methacrylic anhydride was slowly added to the reaction system over a period of time, and the reaction was allowed to proceed for 18 h. After the reaction, the solution was washed with HCl (2 mol/L), saturated $NaHCO_3$ solution, and saturated NaCl solution three times, respectively. The residual water was removed using anhydrous magnesium sulfate. After vacuum evaporation, the crude product was recrystallized with ethyl acetate to get white powder.

Synthesis of Poly (PMA-co-IA-co-MEA) [p(PMA-co-IA-co-MEA)]. In the first step, PMA monomer (2.0624 g, 10 mmol), MEA monomer (0.9761 g, 7.5 mmol), AIBN (0.0328 g), and DMF (10 mL) were simultaneously added into a reaction tube. The mixture was heated to 70 °C under N_2 atmosphere. After 30 min, the IA monomer (0.3443 g, 2.4 mmol) and DMF (5 mL) were added into reaction system. The reaction ended after 12 h.

Synthesis of Poly (PMA-co-MEA). PMA monomer (2.0624 g, 10 mmol), MEA monomer (0.9761 g, 7.5 mmol), AIBN (0.0294 g) and DMF (10 mL) were simultaneously added into a reaction tube. The mixture was heated to 70 °C under N_2 atmosphere. The reaction ended after 12 h.

Synthesis of [methacrylated p(PMA-co-IA-co-MEA)] (MASLU-adhesive). After the p (PMA-co-IA-co-MEA) reaction was completed, the temperature was decreased to 30 °C. HEMA (0.3383 g, 2.6 mmol) and 10 μL DBTDL were dissolved in 2 mL DMF, then added to the reaction system. The mixture reacted for 48 h in the dark. The modified polymer was obtained by washing three times with methyl tert-butyl ether and drying.

Preparation of MWCNTs/SLU-Adhesive Hybrid Material with Photothermal Functionality. The MWCNTs were incorporated into the SLU-adhesive according to the required mass fraction. In order to obtain a homogeneous material, the mixture was ultrasonically dispersed for 1 h, and obtained the MWCNTs/SLU-adhesive hybrid material.

Preparation of MWCNTs/Cotton/SLU-Adhesive Hybrid Material. Cotton was immersed in the above-prepared MWCNTs/SLU-adhesive hybrid material. In order to allow the cotton to inhale sufficient adhesive, the cotton was soaked in the material for 1 h, and obtained the MWCNTs/cotton/SLU-adhesive hybrid material.

Preparation of Sandwich-Structured Hybrid Adhesive Materials of MWCNTs/SLU-Adhesive and PE. The above-prepared MWCNTs/SLU-adhesive hybrid material, was applied to one side of the PE and then immersed them in hot water at 60 °C for 30 min to cure. Next, in the same way, the other side of the PE was coated with the above-prepared MWCNTs/SLU-adhesive hybrid material and immersed in hot water to cure, thus preparing to obtain the sandwich-structured hybrid adhesive materials of MWCNTs/SLU-adhesive and PE. As shown in *SI Appendix*, Fig. S22, the thickness of this material was 280 μm.

Characterizations. The structure of synthesized polymers (water-cured) were characterized by ^{1}H NMR spectrum (400 MHz, Bruker AM-400, Switzerland) in chloroform ($CDCl_3$). Nicolet IS10 FTIR spectrometer (Thermo Fisher Scientific Inc., USA) with a 4-cm^{-1} resolution was used to record the FTIR spectra. The contact

angles were measured at room temperature on an optical contact goniometer (DSA-100 optical CA meter, Kruss Company, Ltd., Germany) after 20 μL drop of deionized water or adhesives was placed carefully on the substrate surface.

SFG Vibrational Spectroscopy. The SFG was acquired employing a commercial SFG system (EKSPLA Inc., Lithuania). In this work, a fused silica right-angled triangular prism was used as the substrate. Teflon was used as a water carrier platform to keep the prism in contact with the water. At this point, the SFG signal of the interfacial water was collected. Then, the adhesive was brought into contact with the prism to remove its interfacial water, and the dynamics of the characteristic signal of the water over time was monitored. Finally, the SFG signal on the prism surface was collected after removing the interfacial water layer.

Rheological Properties Characterization of the Adhesive. The rheological properties of the adhesive were characterized by a oscillatory rheometry (RS6000 HAAKE, Germany) at 25 °C and a frequency sweep (0.01 to 100 Hz) experiment was carried out to examine the storage (G′) and loss (G″) modulus.

Measurement of Surface Roughness. The roughness of stainless steel were characterized by the 3D confocal microscope using an Olympus OLS 5000. Shot using a 500× magnification lens.

Measurement of Underwater Adhesion. Lap-shear test was performed on a WDW-05 electromechanical tester (EZ-Test, SHIMADZU, Japan) to measure the adhesive strength of the adhesive. Before adhesion, the substrates were ultrasonically cleaned in ethanol, and deionized water for 10 min, then completely dried at 30 °C. The lap shear adhesion strength was employed to evaluate the adhesion of the adhesive. The underwater adhesion process was carried out in deionized water. The adhesive was evenly coated on the surface of one substrate, contacted with another substrate under water, and the joint area was recorded. Lap shear adhesion strength tests were performed after immersing the adhesion substrates in water for various times. Likewise, the adhesion strength of samples prepared in different water environments were measured such as seawater and different pH environment. The adhesion strength was calculated as F/S (F is the maximum load and S is the joint area). The crosshead velocity was 20 mm min^{-1}. In each case, at least four samples are tested.

Fluorescence Observation. According to the method similar to the synthesis of p(PMA-co-IA-co-MEA), the fluorescent monomer synthesized above was added to the pre-polymerization solution, and after 12 h of polymerization, the obtained SLU-adhesive contained blue fluorescence. Rhodamine B was dissolved in water to obtain a solution containing yellow fluorescence. The water were dropped on the glass, which spread to form a layer of water film, and 7 μL SLU-adhesive were dropped on it with a syringe. The cover glass was quickly placed on it. Next, the interfacial phenomenon between water and the SLU-adhesive was monitored with a fluorescence microscope (OLYMPUS BX51, Japan).

In Situ Measure the Local Temperature of the SLU-Adhesive Underwater. A thermocouple thermometer was used to measure the underwater temperature. As shown in *SI Appendix*, Fig. S19, the test PI sheets were placed in the water bath, where the water surface was 2.5 cm from the bottom, and the temperature probe was adhered to the bottom of the test PI sheets, which was irradiated with NIR light at a height of 7 cm from the PI sheets. The temperature can be read on the screen of the thermocouple thermometer at different times of irradiation.

Data, Materials, and Software Availability. All study data are included in the article and/or supporting information.

ACKNOWLEDGMENTS. This research was supported by the Strategic Priority Research Program of the Chinese Academy of Sciences (Grant No. XDB 0470200), the National Key Research and Development Program of China (2021YFA0716304), NSAF (Grant No. U2030201), NSF of China (22032006, 22102201, 22072169), Key Research Project of Shandong Provincial Natural Science Foundation (ZR2021ZD27), Gansu Province Basic Research Innovation Group Project (22JR5RA093), Major Program of the Lanzhou Institute of Chemical Physics, Chinese Academy of Sciences (No. ZYFZFX-2), Shandong Laboratory of Yantai Advanced Materials and Green Manufacturing (AMGM0717) and the Special Research Assistant Project of the Chinese Academy of Sciences. We thank Prof. Xiaolin Lu (School of Biological Science & Medical Engineering, Southeast University) for the characterization of sum frequency generation vibrational spectroscopy data.

Author affiliations: [a]State Key Laboratory of Solid Lubrication, Lanzhou Institute of Chemical Physics, Chinese Academy of Sciences, Lanzhou 730000, China; [b]College of Materials Science and Opto-Electronic Technology, University of Chinese Academy of Sciences, Beijing 100049, China; [c]Yantai Zhongke Research Institute of Advanced Materials and Green Chemical Engineering, Shandong Laboratory of Yantai Advanced Materials and Green Manufacturing, Yantai 264006, China; and [d]Department of Materials Science and Engineering, University of California, Los Angeles, CA 90095

1. M. V. Rapp *et al.*, Defining the catechol-cation synergy for enhanced wet adhesion to mineral surfaces. *J. Am. Chem. Soc.* **138**, 9013–9016 (2016).
2. H. L. Fan, J. P. Gong, Bioinspired underwater adhesives. *Adv. Mater.* **33**, 2102983 (2021).
3. H. Yuk *et al.*, Dry double-sided tape for adhesion of wet tissues and devices. *Nature* **575**, 169–174 (2019).
4. Z. Wang, L. F. Guo, H. Y. Xiao, H. Cong, S. T. Wang, A reversible underwater glue based on photo- and thermo-responsive dynamic covalent bonds. *Mater. Horiz.* **7**, 282–288 (2020).
5. C. Y. Cui *et al.*, Water-triggered hyperbranched polymer universal adhesives: From strong underwater adhesion to rapid sealing hemostasis. *Adv. Mater.* **31**, 1905761 (2019).
6. Q. Y. Peng *et al.*, Coacervation-driven instant paintable underwater adhesives with tunable optical and electrochromic properties. *J. Mater. Chem. A* **9**, 12988–13000 (2021).
7. A. Cholewinski, F. Yang, B. X. Zhao, Algae-mussel-inspired hydrogel composite glue for underwater bonding. *Mater. Horiz.* **6**, 285–293 (2019).
8. Q. Zhao *et al.*, Underwater contact adhesion and microarchitecture in polyelectrolyte complexes actuated by solvent exchange. *Nat. Mater.* **15**, 407–412 (2016).
9. Q. Zhang *et al.*, Formation of a supramolecular polymeric adhesive via water-participant hydrogen bond formation. *J. Am. Chem. Soc.* **141**, 8058–8063 (2019).
10. S. Liang *et al.*, Paintable and rapidly bondable conductive hydrogels as therapeutic cardiac patches. *Adv. Mater.* **30**, 1704235 (2018).
11. Y. H. Zhao *et al.*, Bio-inspired reversible underwater adhesive. *Nat. Commun.* **8**, 2218 (2017).
12. H. L. Fan *et al.*, Adjacent cationic-aromatic sequences yield strong electrostatic adhesion of hydrogels in seawater. *Nat. Commun.* **10**, 5127 (2019).
13. X. Y. Li *et al.*, Coassembly of short peptide and polyoxometalate into complex coacervate adapted for pH and metal ion-triggered underwater adhesion. *Langmuir* **35**, 4995–5003 (2019).
14. J. Xu *et al.*, Wet and functional adhesives from one-step aqueous self-assembly of natural amino acids and polyoxometalates. *Angew. Chem. Int. Ed.* **56**, 8731–8735 (2017).
15. J. Sun *et al.*, Genetically engineered polypeptide adhesive coacervates for surgical applications. *Angew. Chem. Int. Ed.* **60**, 23687–23694 (2021).
16. H. Liu *et al.*, Bio-inspired self-hydrophobized sericin adhesive with tough underwater adhesion enables wound healing and fluid leakage sealing. *Adv. Funct. Mater.* **32**, 2201108 (2022).
17. X. Liu, Q. Zhang, L. J. Duan, G. H. Gao, Bioinspired nucleobase-driven nonswellable adhesive and tough gel with excellent underwater adhesion. *ACS Appl. Mater. Interfaces* **11**, 6644–6651 (2019).
18. Q. T. Song *et al.*, Adhesive capable of underwater adhesion and wound hemostasis prepared based on solvent exchange. *Adv. Mater. Technol.* **7**, 2100852 (2022).
19. L. J. Xu *et al.*, A solvent-exchange strategy to regulate noncovalent interactions for strong and antiswelling hydrogels. *Adv. Mater.* **32**, 2004579 (2020).
20. X. Su *et al.*, Strong underwater adhesion of injectable hydrogels triggered by diffusion of small molecules. *Mater. Horiz.* **8**, 2199–2207 (2021).
21. H. L. Fan, J. H. Wang, J. P. Gong, Barnacle cement proteins-inspired tough hydrogels with robust, long-lasting, and repeatable underwater adhesion. *Adv. Funct. Mater.* **31**, 2009334 (2021).
22. X. W. Zhu *et al.*, A cation-methylene-phenyl sequence encodes programmable poly(ionic liquid) coacervation and robust underwater adhesion. *Adv. Funct. Mater.* **32**, 2105464 (2022).
23. H. L. Fan, Y. R. Cai, J. P. Gong, Facile tuning of hydrogel properties by manipulating cationic-aromatic monomer sequences. *Sci. China-Chem.* **64**, 1560–1568 (2021).
24. Y. G. Yan *et al.*, A strong underwater adhesive that totally cured in water. *Chem. Eng. J.* **431**, 133460 (2022).
25. G. Z. Xia *et al.*, Solvent-free mussel-inspired adhesive with rapid underwater curing capability. *Adv. Mater. Interfaces* **8**, 2101544 (2021).
26. Y. Akdogan *et al.*, Intrinsic surface-drying properties of bioadhesive proteins. *Angew. Chem. Int. Ed. Engl.* **53**, 11253–11256 (2014).
27. N. Poulsen *et al.*, Isolation and biochemical characterization of underwater adhesives from diatoms. *Biofouling* **30**, 513–523 (2014).
28. F. L. Zhang, X. B. Jiang, X. L. Zhu, Z. Y. Chen, X. Z. Kong, Preparation of uniform and porous polyurea microspheres of large size through interfacial polymerization of toluene diisocyanate in water solution of ethylene diamine. *Chem. Eng. J.* **303**, 48–55 (2016).
29. J. Lukaszczyk, P. Urbas, Influence of the parameters of encapsulation process and of the structure of diisocyanates on the release of codeine from resinate encapsulated in polyurea by interfacial water promoted polyreaction. *React. Funct. Polym.* **33**, 233–239 (1997).
30. B. Rehl, J. M. Gibbs, Role of ions on the surface-bound water structure at the silica/water interface: Identifying the spectral signature of stability. *J. Phys. Chem. Lett.* **12**, 2854–2864 (2021).
31. J. R. Hollahan, G. L. Carlson, Hydroxylation of polymethylsiloxane surfaces by oxidizing plasmas. *J. Appl. Polym. Sci.* **14**, 2499–2508 (1970).
32. S. W. Wu *et al.*, Heterogeneous ice nucleation correlates with bulk-like interfacial water. *Sci. Adv.* **5**, eaat9825 (2019).
33. Z. Wang *et al.*, Facile biomimetic self-coacervation of tannic acid and polycation: Tough and wide pH range of underwater adhesives. *Chem. Eng. J.* **404**, 127069 (2021).

34. Y. Xu *et al.*, Mussel-inspired polyesters with aliphatic pendant groups demonstrate the importance of hydrophobicity in underwater adhesion. *Adv. Mater. Interfaces* **4**, 1700506 (2017).
35. H. Shao, R. J. Stewart, Biomimetic underwater adhesives with environmentally triggered setting mechanisms. *Adv. Mater.* **22**, 729–733 (2010).
36. Z. L. Wu, L. Li, Y. B. Mu, X. B. Wan, Synthesis and adhesive property study of a mussel-inspired adhesive based on poly(vinyl alcohol) backbone. *Macromol. Chem. Phys.* **218**, 1700206 (2017).
37. C. Y. Wei *et al.*, Facile preparation of lignin-based underwater adhesives with improved performances. *ACS Sustain. Chem. Eng.* **7**, 4508–4514 (2019).
38. C. Y. Sun *et al.*, Water-resistant and underwater adhesive ion-conducting gel for motion-robust bioelectric monitoring. *Chem. Eng. J.* **431**, 134012 (2022).
39. Q. Y. Peng *et al.*, Coacervate-based instant and repeatable underwater adhesive with anticancer and antibacterial properties. *ACS Appl. Mater. Interfaces* **13**, 48239–48251 (2021).
40. Y. Li *et al.*, A bio-inspired multifunctional soy protein-based material: From strong underwater adhesion to 3D printing. *Chem. Eng. J.* **430**, 133017 (2022).
41. X. D. Li *et al.*, Bringing hetero-polyacid-based underwater adhesive as printable cathode coating for self-powered electrochromic aqueous batteries. *Adv. Funct. Mater.* **28**, 1800599 (2018).
42. A. Li *et al.*, Mineral-enhanced polyacrylic acid hydrogel as an oyster-inspired organic-inorganic hybrid adhesive. *ACS Appl. Mater. Interfaces* **10**, 10471–10479 (2018).
43. R. G. Arnold, J. A. Nelson, J. J. Verbanc, Recent advances in isocyanate chemistry. *Chem. Rev.* **57**, 47–76 (1957).
44. H. Y. Feng *et al.*, Reversing hydrogel adhesion property via firmly anchoring thin adhesive coatings. *Adv. Funct. Mater.* **32**, 2111278 (2022).